Copyright © 2006 American Scientific Publishers
All rights reserved
Printed in the United States of America

Journal of
Computational and Theoretical Nanoscience
Vol. 3, 118–127, 2006

# Adaptive Tempering Monte Carlo Method

Xiao Dong and Estela Blaisten-Barojas*

*School of Computational Sciences, George Mason University, Fairfax, Virginia 22030-4422, USA*

The Adaptive Tempering Monte Carlo (ATMC) optimization method based on multi-canonical Monte Carlo is proposed in this work to optimize the preferred structure of atomic clusters. The method also works well to obtain the structure of solid crystals at low temperatures resulting from an annealing process. The weights that link the sub-canonical ensembles are adapted progressively during the simulation. The method was tested on Morse atomic clusters containing 10–155 atoms, for which the global minimum structures were obtained at the end of quenches from high temperature to zero temperature. A second example was the structural optimization of quantum tight-binding clusters of calcium containing 13 to 32 atoms. A third example is the solidification of a Lennard-Jones liquid system, which yielded a crystal with few defects in a single pass of the tempering method. The ATMC proves to be very efficient for optimization of ordered structures, and can be used in classical and quantum approaches.

**Keywords:** Computational Nanomaterials Design, Calcium Nanoclusters, Morse Nanoclusters, Monte Carlo, Multicanonical, Tempering, Structural Optimization, Tight-Binding.

## 1. INTRODUCTION

In the last few years there has been a lot of interest around different implementations of the simulated tempering method proposed individually by Marinari and Parisi[1] and by Lyubartsev et al.[2] The method involves the construction of a Markov chain of configurational energies in which $E_A(T_A)$ is linked to $E_B(T_B)$, where $A$ and $B$ identify two different partition functions of the same type of statistical mechanics ensembles at two temperatures $T_A$ and $T_B$. The new sampling distribution characterizes an expanded ensemble. If there are $n$ of such partition functions, the expanded ensemble is obtained from the following partition function:

$$Z = \sum_{i=1}^{n} Z_i \exp(-\eta_i) \tag{1}$$

where $Z_i$ is the partition function associated with the sampling distribution of a standard NVT ensemble and $\eta_i$ are weights. Each $Z_i$ is usually referred as sub-ensemble of the expanded ensemble. The basic idea is to construct $Z$ so that the corresponding sampling distribution explores all the regions of configuration space 'containing' evenly regions associated to two phase-constrained distributions and the regions in between them. This approach also bears other names, i.e., simulated tempering,[3] umbrella sampling,[4] multicanonical,[5] just to mention a few. For the case $\pi_i$ representing the Gibbs canonical ensemble NVT of a system of $N$ particles and Hamiltonian $H(\mathbf{q})$, each $Z_i$ is

$$Z_i = \frac{1}{N!}\int \exp(-H(\mathbf{q})/k_B T_i)d\mathbf{q} \tag{2}$$

where $k_B$ is Boltzmann's constant. If $\pi_i$ is the Gibbs distribution, the usual particle displacement to yield a configuration at temperature $T_i$ with the Metropolis acceptance criterion:

$$acc = \min[1, \exp-(H(\mathbf{q}_{\mathbf{new}}) - H(\mathbf{q}_{\mathbf{old}}))/k_B T_i] \tag{3}$$

is adopted for sub-ensemble $i$. In the simulation it is necessary to consider a second type of MC-move, which attempts to change sub-ensembles, i.e. from $m$ to $m'$ such that this move keeps the effective configuration $\mathbf{q}$ constant whilst attempting to change the sampling distribution from $\pi_m = Z_m\exp(-\eta_m)/Z$ to $\pi_{m'} = Z_{m'}\exp(-\eta_{m'})/Z$. Generally $m'$ is chosen to be an adjacent sub-ensemble of $m$. In order to satisfy detailed balance and in order to yield a sampling distribution with a partition function given by Eq. (1), such a move must be accepted with probability:

$$acc = \min\left[1, \frac{e^{-(H(\mathbf{q})/k_B T_{m'} + \eta_{m'})}}{e^{-(H(\mathbf{q})/k_B T_m + \eta_m)}}\right] \tag{4}$$

Under the sampling distributions $\pi_m$ and $\pi_{m'}$ it follows that the ratio of the probabilities of the simulation being found in these two sub-ensembles is given by:

$$\frac{\pi_m}{\pi_{m'}} = \frac{Z_m}{Z_{m'}} e^{-(\eta_m - \eta_{m'})} \tag{5}$$

---

*Author to whom correspondence should be addressed.

1546-198X/2006/3/118/010 doi:10.1166/jctn.2006.010

Since the ratio of the probabilities of finding the simulation in two sub-ensembles is estimated by the ratio of the times spent in the two sub-ensembles, one can determine an estimate for the ratio between partition functions by means of an estimator $R_{m,m'}$. By hopping between the sub-ensembles the simulation is able to explore a wider region of an effective configuration space than it would under a sampling experiment performed with any one of the individual sampling distributions $\pi_m$. In order to ensure that the simulation visits all requested sub-ensembles, one must first ensure that sufficient intermediate sub-ensembles have been constructed to allow for distribution overlaps. One must also ensure that the correct weights $\eta_m$ have been chosen so as to guarantee that the simulation is able to frequently traverse between the regions of (effective) configuration space typically associated with phase A and those typically associated with phase B. One way to do this is to choose the weights so that equal times are spent in all the sub-ensembles. In this case one sets $\eta_i = ln(Z_i) = constant$. However since *a priori* the partition functions are not known, it follows that the weights must be constructed in an iterative fashion, i.e. via the visited states method or the Wang-Landau method,[6,7] as is done in the Umbrella Sampling method.[4,5] Having obtained the weights one may then proceed to estimate the ratio of the partition functions by appeal to the estimator $R_{m,m'}$. Customarily, this $R_{m,m'}$ for $NVT$ systems is done through three types of strategies: the reference state technique, the continuous phase technique, and the phase mapping technique.

Lyubartsev et al.[2] reached Eqs. 1–5 by defining an effective Hamiltonian containing the weights $\eta_m$, $H(\mathbf{q})_m = H(\mathbf{q})/k_B T_m + \eta_m$. These effective Hamiltonians lead to Gibbs distribution for fixed $i$, such that a conventional Metropolis acceptance strategy can be used, although two types of MC moves are also involved. These authors relate the differences in weights $\eta$ to differences in free energy and use the ideal gas at high temperatures as the reference system.

The optimization of the best structure of atomic clusters is difficult because of the multitude of geometries associated with isomers, which have energies very close to each other. This problem is encountered in both classical and quantum mechanical methods to represent the total energy of the system at zero temperature. In this paper we propose a simulation method that permits to optimize cluster structures, and that can be either linked to calculation of energies through classical approaches based on model potentials or to a quantum tight-binding approach. The process is the Adaptive Tempering Monte Carlo (ATMC) method that we describe in Section 2. Section 3 of this paper describes the results for Morse clusters containing 80 to 150 atoms. Section 4 gives an overview of the combination of the ATMC with the tight binding (TB) calculation of the energy of calcium clusters containing 13 to 32 atoms. The TB model used was discussed in a previous paper.[8] In Section 5 we discuss the use of the ATMC for infinite systems, and the example is the crystallization of Lennard Jones liquids. This paper is concluded in Section 6 with summarizing remarks.

## 2. THE ADAPTIVE TEMPERING MONTE CARLO

In the Adaptive Tempering MC method (ATMC), the system accesses a multitude of $NVT_i$ ensembles, where each $T_i$ characterizes a different ensemble within a predetermined temperature range. The set of temperatures $T_i$ is not necessarily associated to two phases of the system. Each canonical ensemble is simulated with the Metropolis acceptance criterion of Eq. (3) for a fixed number of configuration changes $M_{\text{fixed}}$ with a variable step size to roughly accept 50% of configuration changes and reject 50%. The various ensembles are connected along the simulation by a super-Markov chain in which for $\Delta T > 0$, the temperature $T$ is allowed to hop to either $T + \Delta T$ or $T - \Delta T$ with the following probabilities:

$$\pi_+ = \exp\left[-(E - \langle E\rangle)\left(\frac{1}{k_B(T+\Delta T)} - \frac{1}{k_B T}\right)\right]\Big/ Q \quad (6)$$

$$\pi_- = \exp\left[-(E - \langle E\rangle)\left(\frac{1}{k_B(T-\Delta T)} - \frac{1}{k_B T}\right)\right]\Big/ Q \quad (7)$$

where $E$ is the $M_{\text{fixed}}^{\text{th}}$ instantaneous configuration energy at $T$, $\langle E\rangle$ is the MC average energy of the $M_{\text{fixed}}$ configurations, and the normalization factor $Q$ is such that $\pi_+ + \pi_- = 1$. After some rearrangements, these probabilities can be rewritten as:

$$\pi_+ = e^{\left[\frac{E-\langle E\rangle}{k_B T_{\text{adapt}}}\right]}/Q_{\text{adapt}} \quad (8)$$

$$\pi_- = e^{\left[-\frac{E-\langle E\rangle}{k_B T_{\text{adapt}}}\right]}/Q_{\text{adapt}} \quad (9)$$

where

$$Q_{\text{adapt}} = 2\cosh((E - \langle E\rangle)/k_B T_{\text{adapt}}) \quad (10)$$

and where

$$T_{\text{adapt}} = (T^2 - \Delta T^2)/\Delta T \quad (11)$$

is an adaptive local temperature. An estimate of this adaptive local temperature is obtained from $\Delta T$:

$$\Delta T = \frac{T}{1 - \delta E/(ln(a) k_B T)} \quad (12)$$

Here $\delta E$ is the standard deviation of the energy about the average $\langle E\rangle$ at temperature $T$ over the $M_{\text{fixed}}$ configuration trials. We introduce one parameter $ln(a)$ in terms of which $T_{\text{adapt}}$ is readily obtained. In the following sections we give several examples with the optimal value of $ln(a)$ in each case. This algorithm enables the system to visit a wide range of temperatures. Every time that the temperature *hops* to a new temperature, we say that a tempering event took place. Subsequently, the system evolves for another $M_{\text{fixed}}$ set of configurations satisfying Eq. (3) at either $T+\Delta T$ or $T-\Delta T$. In all simulations the system is started from an arbitrary initial configuration at high temperatures close to the upper limit of the allowed temperature range. The simulation is stopped when the temperature is close to zero. The energy $E$ is calculated consistent with the model used to simulate the system, which is not restricted to be a classical energy from a model potential. Additionally, the adaptive tempering algorithm might be easily combined with other ways to calculate $\langle E\rangle$ and $\delta E$, such as molecular dynamics or Langevin dynamics and is not necessarily an exclusive MC method.

In the ATMC, the system spends equal times in all the sub-ensembles. In Eq. (6), the weights $\eta$ are locally assigned an adaptive constant based on the local $T$, and the fact that three sub-ensembles are considered at each tempering step, i.e., the actual sub-ensemble $NVT$ and the two neighboring sub-ensembles $NV(T\pm\Delta T)$. Therefore,

$$\eta_{\pm} = ln(Z_{\pm}) = \pm(E-\langle E\rangle)/k_B T_{\text{adapt}} \cong |E-\langle E\rangle|/(3k_B T) \tag{13}$$

The practical implementation of the ATMC is simple. An NVT Metropolis MC with adaptive step size is run for $M_{\text{fixed}}$ steps at the initial temperature $T$. The $\langle E\rangle$ and $\delta E$ are calculated and $E$ of the $M_{\text{fixed}}^{\text{th}}$ is known. Next, $\Delta T$ is calculated from Eq. (12) and one of the two probabilities $\pi_+$ or $\pi_-$ is selected when its numerator in Eq. (6) or Eq. (7) is $<1$. A random number uniformly distributed (0,1) is thrown. If the chosen $\pi$ is larger than the random number, the temperature is changed consistent with the chosen $\pi$. If the chosen $\pi$ is smaller than the random number, then the other $\pi$ is selected. In either case, the temperature is changed and the new temperature is $T+\Delta T$ or $T-\Delta T$. Subsequently the Metropolis MC simulation is restarted from the known $M_{\text{fixed}}^{\text{th}}$ configuration but now at the new temperature. New values of $\langle E\rangle$, $\delta E$, and $E$ are calculated at the end of another set of $M_{\text{fixed}}$ steps. A new $\Delta T$ is calculated, and the above-discussed process is repeated to select another new temperature. This adaptive process is continued until the system reaches a final temperature close to zero, at which point the simulation stops. Would the simulation be continued, it would reach negative temperatures, and basically does not return to high temperatures once the ground state is reached.

The ATMC is not a parallel algorithm. However, parallelization can be achieved effectively at the implementation level. For example, using the Portland Group compiler,[9] the speedup on our shared memory parallel machine is almost perfect. The advantage of ATMC over other tempering implementations such as the replica exchange parallel algorithm of Ref. [10] is that no synchronization is required between the processes associated to each of the tempering events. The ATMC removes this rigid requirement.

## 3. CLASSICAL ATMC: MORSE NANOCLUSTERS

Several materials have been modeled under the Morse potential. This model potential, and combination of several of them, is extensively used in the embedded atom model. When used to model clusters, the structures of lowest energy change with the softness of this potential. This characteristic was emphasized in the past, and the value of the parameter associated to the repulsion at short distances ($\rho$) has been reported for several metals.[11] For clusters containing $N$ atoms, a concise database[12] contains the structural information of known preferred geometries for up to $N=80$. We used the ATMC to search for the energetically preferred structures of larger Morse clusters. These clusters are in the nanometer size domain containing 81 to 155 atoms.

The calculations were done in reduced units of the Morse parameters $D_e$ for energy and $r_e$ for distances. Then, the total binding energy $E$ of a cluster with $N$ atoms is

$$E_N = \sum_{i=1}^{N}\sum_{j<i}^{N}\left[e^{\rho(1-r_{ij})}\left(e^{\rho(1-r_{ij})}-2\right)+\alpha(r_{ij}/r_{cage})^{14}\right] \tag{14}$$

where $r_{ij}$ are the distances between atoms in the cluster. The first term corresponds to the Morse potential, and the second term is a cage potential with central symmetry added to maintain the atoms inside a spherical volume of radius $r_{\text{cage}}$. For this calculation we used two values of the Morse parameter $\rho=3.0$ and 3.68. Additionally, $\alpha=1.0\times10^{-4}$ and $r_{\text{cage}}$ was chosen to be roughly twice the maximum distance between atoms in the initial configuration of each cluster. Temperature is in units of $D_e/k_B$. The best values of the two ATMC parameters are $M_{\text{fixed}}=100$ and $ln(a)=-0.7$ and the ATMC process was started for all sizes at about $T=0.5$ and various initial configurations corresponding to Lennard Jones (LJ) clusters with the same number of atoms, spherical cuts from the fcc lattice, or other previous configurations. Figure 1 illustrates the evolution of the temperature and the binding energy as a function of tempering event for a cluster with $N=116$ atoms. There are 2120 tempering events in this case, showing clearly that the cluster is visiting a vast region of configuration space. The correlation between visited energies and accepted temperatures is shown in Figure 1c, which suggests an almost linear temperature-energy correlation along each of the two phases accessed along the tempering.

Table I contains binding energies and point groups of the preferred structures for the case $\rho=3.0$ discovered by the ATMC. Table II summarizes the same quantities for the case $\rho=3.6$. Values reported in the third column of these tables correspond to the pure Morse binding energy (first term of Eq. 14) once the final structure from the ATMC process has been locally minimized. This binding energy as a function of size is plotted in Figure 2a (empty circles). As expected, the binding energy per atom has a steady increase with increasing size. Figure 2a also illustrates the

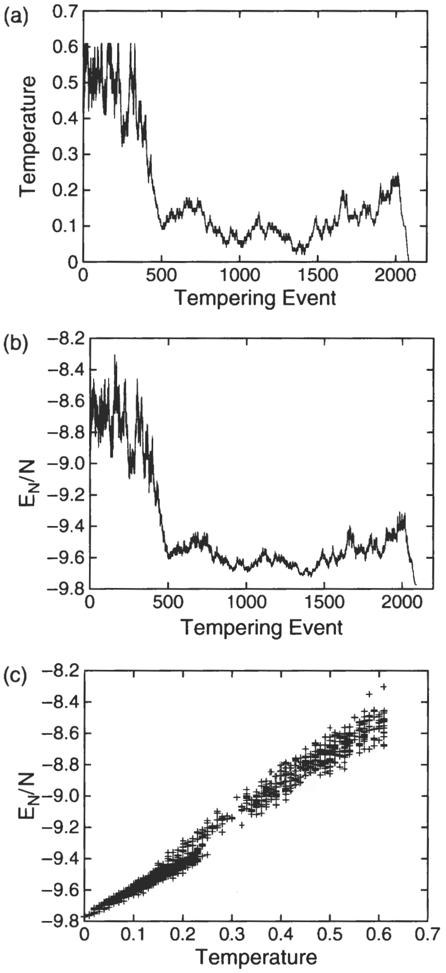

**Fig. 1.** Evolution of the temperature (a) and the energy (b) as a function of tempering event for the 116-atom Morse cluster ($\rho = 3.0$); (c) correlation between energy and temperature during the tempering process. Energies are in reduced units of $D_e$ and temperatures in units of $D_e/K_B$.

energies for clusters in the size range 10 to 80 (black circles) already reported in the literature.[12] The large clusters tend to have low symmetry; for the case $\rho = 3.0$ $N = 110$, 116, 121, 148 and for the case $\rho = 3.68$ $N = 116$, 136, 141 are exceptions with point group $C_5$. Additionally, for the later $N = 91$ is $D_5$ cluster and $N = 135$, 147 are $I_h$. In Figures 2b, c we report the stability pattern of these clusters given by the second difference of the binding energy $\Delta_2$

$$\Delta_2 = E_{N-1} - 2\,E_N + E_{N+1} \tag{15}$$

The $\Delta_2$ is used to determine the relative stability of clusters, indicating that sizes corresponding to peaks are relatively more stable than the neighboring sizes. Based on this analysis, the more stable clusters in the newly studied size range are 105, 110, 115, 142, and 152 for the case of $\rho = 3.0$ and 105, 115, 135, and 147 for the $\rho = 3.68$ case. The later shares the same magic number $N = 147$ with the Lennard Jones clusters,[13] which is a MacKay icosahedron. Additionally the Morse $N = 135$ cluster with $I_h$ symmetry is an energetically preferred structure, whereas the Lennard Jones cluster of that size is not a magic number but has the same structure.

**Table I.** Morse clusters with $\rho = 3.0$: binding energy per atom (in units of $D_e$) and the corresponding point group.

| $N$ | Energy/$N$ | | $N$ | Energy/$N$ | | $N$ | Energy/$N$ | |
|---|---|---|---|---|---|---|---|---|
| 81 | −8.6683 | $C_2$ | 106 | −9.4533 | $C_1$ | 131 | −10.0710 | $C_1$ |
| 82 | −8.7019 | $C_1$ | 107 | −9.4815 | $C_1$ | 132 | −10.0916 | $C_1$ |
| 83 | −8.7397 | $C_2$ | 108 | −9.5100 | $C_2$ | 133 | −10.1119 | $C_3$ |
| 84 | −8.7731 | $C_1$ | 109 | −9.5371 | $C_1$ | 134 | −10.1306 | $C_1$ |
| 85 | −8.8076 | $C_1$ | 110 | −9.5848 | $D_5$ | 135 | −10.1549 | $C_1$ |
| 86 | −8.8418 | $C_1$ | 111 | −9.6074 | $C_1$ | 136 | −10.1770 | $C_1$ |
| 87 | −8.8731 | $C_1$ | 112 | −9.6345 | $C_1$ | 137 | −10.1983 | $C_1$ |
| 88 | −8.9052 | $C_1$ | 113 | −9.6688 | $C_3$ | 138 | −10.2189 | $C_1$ |
| 89 | −8.9369 | $C_2$ | 114 | −9.7040 | $C_1$ | 139 | −10.2371 | $C_1$ |
| 90 | −8.9716 | $C_5$ | 115 | −9.7522 | $C_1$ | 140 | −10.2743 | $C_1$ |
| 91 | −8.9997 | $C_1$ | 116 | −9.7742 | $C_5$ | 141 | −10.3103 | $C_5$ |
| 92 | −9.0355 | $C_1$ | 117 | −9.7962 | $C_2$ | 142 | −10.3275 | $C_2$ |
| 93 | −9.0638 | $C_1$ | 118 | −9.8183 | $C_3$ | 143 | −10.3457 | $C_1$ |
| 94 | −9.0962 | $C_2$ | 119 | −9.8400 | $C_2$ | 144 | −10.3637 | $C_2$ |
| 95 | −9.1291 | $C_1$ | 120 | −9.8614 | $C_1$ | 145 | −10.3807 | $C_1$ |
| 96 | −9.1591 | $C_2$ | 121 | −9.8827 | $C_5$ | 146 | −10.4000 | $C_1$ |
| 97 | −9.1875 | $C_1$ | 122 | −9.9033 | $C_1$ | 147 | −10.4184 | $C_1$ |
| 98 | −9.2171 | $C_1$ | 123 | −9.9239 | $C_2$ | 148 | −10.4373 | $D_2$ |
| 99 | −9.2457 | $C_1$ | 124 | −9.9441 | $C_3$ | 149 | −10.4556 | $C_3$ |
| 100 | −9.2734 | $C_1$ | 125 | −9.9640 | $C_2$ | 150 | −10.4730 | $C_2$ |
| 101 | −9.3015 | $C_1$ | 126 | −9.9839 | $C_5$ | 151 | −10.4900 | $C_1$ |
| 102 | −9.3221 | $C_2$ | 127 | −10.0039 | $C_1$ | 152 | −10.5079 | $C_1$ |
| 103 | −9.3581 | $C_1$ | 128 | −10.0205 | $C_3$ | 153 | −10.5308 | $C_1$ |
| 104 | −9.3845 | $C_3$ | 129 | −10.0333 | $C_1$ | 154 | −10.5628 | $D_3$ |
| 105 | −9.4308 | $D_3$ | 130 | −10.0516 | $C_2$ | 155 | −10.5779 | $C_1$ |

Interesting to note is the fact that in the Morse nanoclusters with very soft repulsive wall of $\rho = 3.0$, the

**Table II.** Morse clusters with $\rho = 3.68$: binding energy per atom (in units of $D_e$) and the corresponding point group.

| $N$ | Energy/$N$ | | $N$ | Energy/$N$ | | $N$ | Energy/$N$ | |
|---|---|---|---|---|---|---|---|---|
| 81 | −6.5494 | $C_2$ | 106 | −6.9240 | $C_1$ | 131 | −7.2197 | $C_1$ |
| 82 | −6.5594 | $C_3$ | 107 | −6.9372 | $C_1$ | 132 | −7.2232 | $C_1$ |
| 83 | −6.5792 | $C_1$ | 108 | −6.9460 | $C_1$ | 133 | −7.2310 | $C_1$ |
| 84 | −6.5966 | $C_1$ | 109 | −6.9586 | $C_1$ | 134 | −7.2526 | $C_1$ |
| 85 | −6.6186 | $C_3$ | 110 | −6.9740 | $C_1$ | 135 | −7.2862 | $I_h$ |
| 86 | −6.6358 | $C_1$ | 111 | −6.9862 | $C_1$ | 136 | −7.2945 | $C_5$ |
| 87 | −6.6568 | $C_1$ | 112 | −7.0078 | $C_1$ | 137 | −7.3027 | $C_{2v}$ |
| 88 | −6.6673 | $C_1$ | 113 | −7.0299 | $C_1$ | 138 | −7.3108 | $C_3$ |
| 89 | −6.6864 | $C_1$ | 114 | −7.0516 | $C_1$ | 139 | −7.3187 | $C_{2v}$ |
| 90 | −6.6983 | $C_1$ | 115 | −7.0836 | $C_1$ | 140 | −7.3265 | $C_s$ |
| 91 | −6.7159 | $D_5$ | 116 | −7.0931 | $C_5$ | 141 | −7.3342 | $C_5$ |
| 92 | −6.7283 | $C_1$ | 117 | −7.1024 | $C_2$ | 142 | −7.3418 | $C_s$ |
| 93 | −6.7456 | $C_1$ | 118 | −7.1116 | $C_3$ | 143 | −7.3493 | $C_{2v}$ |
| 94 | −6.7638 | $C_1$ | 119 | −7.1205 | $C_2$ | 144 | −7.3567 | $C_3$ |
| 95 | −6.7727 | $C_1$ | 120 | −7.1292 | $C_1$ | 145 | −7.3639 | $C_{2v}$ |
| 96 | −6.7898 | $C_1$ | 121 | −7.1377 | $C_3$ | 146 | −7.3711 | $C_5$ |
| 97 | −6.7980 | $C_1$ | 122 | −7.1460 | $C_1$ | 147 | −7.3781 | $I_h$ |
| 98 | −6.8110 | $C_1$ | 123 | −7.1541 | $C_2$ | 148 | −7.3751 | $C_s$ |
| 99 | −6.8231 | $C_1$ | 124 | −7.1620 | $C_3$ | 149 | −7.3808 | $D_3$ |
| 100 | −6.8422 | $C_1$ | 125 | −7.1697 | $C_{2v}$ | 150 | −7.3870 | $C_1$ |
| 101 | −6.8571 | $C_1$ | 126 | −7.1796 | $C_5$ | 151 | −7.3974 | $C_s$ |
| 102 | −6.8721 | $C_1$ | 127 | −7.1881 | $C_1$ | 152 | −7.4037 | $C_1$ |
| 103 | −6.8910 | $C_1$ | 128 | −7.1965 | $C_1$ | 153 | −7.4104 | $C_1$ |
| 104 | −6.9051 | $C_1$ | 129 | −7.2047 | $C_1$ | 154 | −7.4184 | $C_3$ |
| 105 | −6.9187 | $C_1$ | 130 | −7.2126 | $C_1$ | 155 | −7.4229 | $C_1$ |

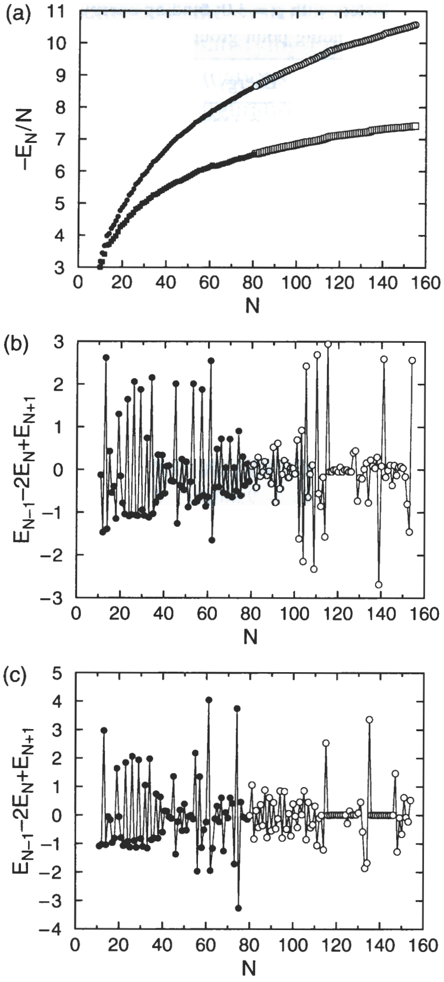

**Fig. 2.** Morse clusters: (a) Binding energy per atom of Morse clusters as a function of size; (b) Stability pattern as a function of size for $\rho = 3.0$; (c) Stability pattern as a function of size for $\rho = 3.68$. Energies are in reduced units of $D_e$.

internal atoms are quasi-bounded to their neighbors. For example, the $N = 82$ cluster has 28 internal atoms with positive pair interactions with several neighbors. Therefore these atoms are rattling inside the cluster. This effect might be the source for the low symmetry characteristics of the Morse nanoclusters with low values of $\rho$. For a cluster of the same size, but $\rho = 3.68$, all interatomic interactions are negative and the cluster has a higher symmetry of $C_3$. Figure 3 shows a comparison of the pair distribution functions of the Morse $N = 82$ cluster and that of the magic number of calcium clusters $Ca_{82}$ ($D_{3d}$) within the tight binding approximation.[8] The first-neighbor interatomic distances in the Morse cluster with $\rho = 3.0$ peaks at $r = 0.8003$. At this interatomic distance the pair potential is zero, which indicates that most atoms are not bound to the shell of first neighbors, but rather the external shells keep the cluster together. The first-neighbor peak shifts to $r = 0.9311$ for the Morse potential with $\rho = 3.68$, for which the pair interactions are now all negative. However, when compared to the tight binding result for $Ca_{82}$, it is seen that the second-neighbor distances are in agreement, but the first coordination shell is compressed in the case of the Morse cluster.

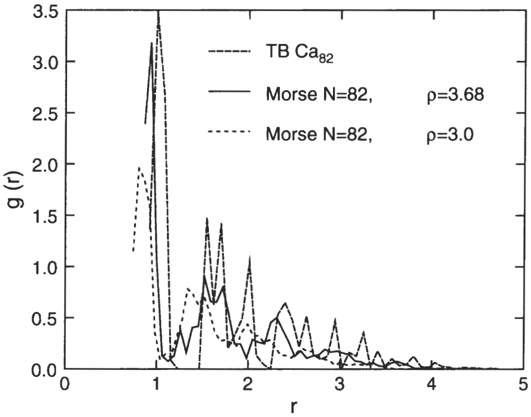

**Fig. 3.** Comparison of the pair correlation function of the optimized $N = 82$ cluster with Morse potential $\rho = 3.0$ (dotted line) and $\rho = 3.68$ (solid line) with the optimized calcium $Ca_{82}$ cluster with the tight binding model (dashed line). Distances are reported in units of $r_o$ for the Morse case and with $r_o = 3.8213$ Å for the TB case.

The results in this section were collected from 16 ATMC runs for all cluster sizes done in parallel using 16 processors. The repeat process was necessary to verify that the optimized structures were repetitive. Discrepancies between different runs did not exceed four structures. As a further verification of the ATMC we optimized Lennard Jones (LJ) clusters containing 10–150 atoms, and again, the known structures were reproduced in just one passage of the ATMC. The ATMC parameters for LJ clusters were the same than those used for the Morse clusters.

## 4. QUANTUM ATMC: TIGHT BINDING CLUSTERS

The TB model and parameters adopted to obtain the binding energy $E$ were previously used by the authors in Ref. [8] where readers are referred for details. The model is based on the Slater-Koster (SK) approach[14] in which $s$, $p$, and $d$ orbitals span a $9 \times 9$ matrix representation of the TB Hamiltonian for each atom in the cluster. The basis set is non-orthogonal and the model has 97 parameters associated to the analytical representation of on-site and hopping integrals. These parameters were fitted to the energy bands and cohesive energy of bulk fcc and bcc calcium[15] and to the *ab initio* energy surfaces[16] of $Ca_7$ through $Ca_{13}$ and are reported in Ref. [8].

The two ATMC parameters were set to $M_{\text{fixed}} = 100$ and $ln(a) = -2$.[17] The starting cluster configurations are spherical cuts from a simple cubic lattice. Before the tempering starts, any given cluster is warmed up for 10,000 iterations of a regular canonical ensemble MC at temperature $T = 800$ K. At this point the adaptive tempering starts, and the system adaptively changes temperature until the $T_{\text{new}}$ reaches the desired lower limit, which was $\sim$1 K.

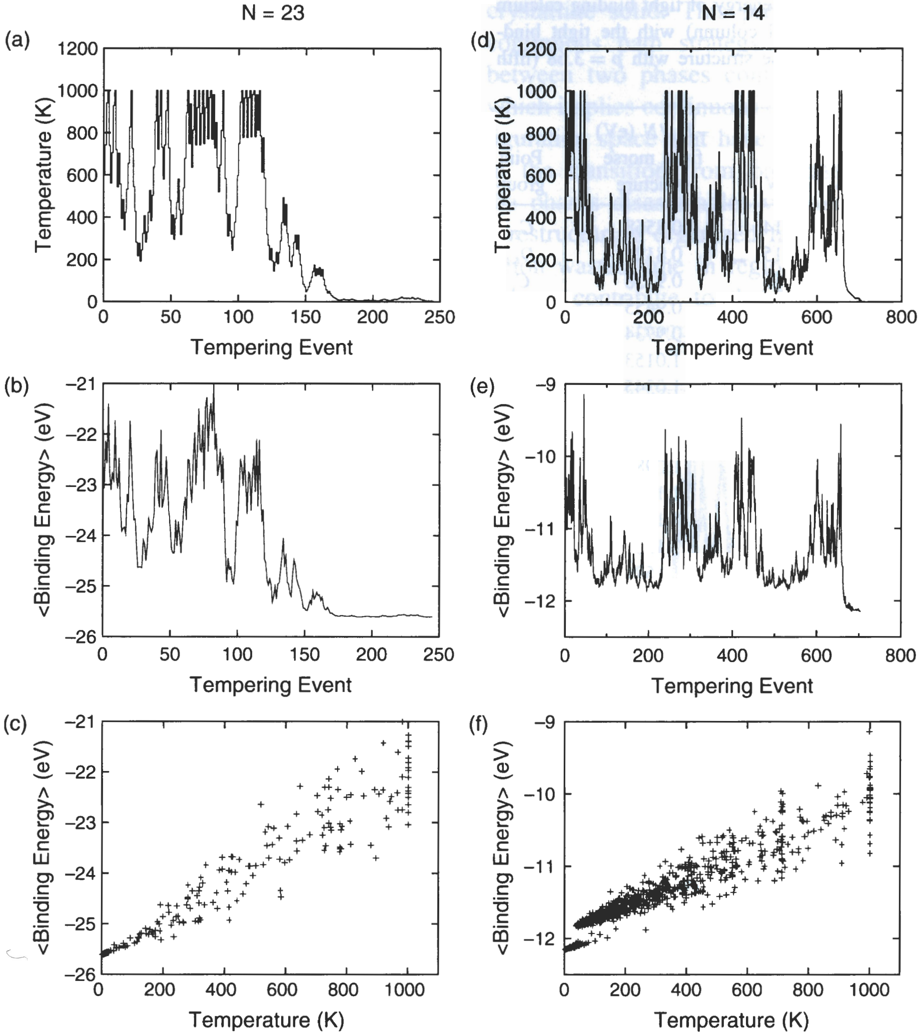

**Fig. 4.** Temperature and average binding energy along the ATMC simulation. (a), (b), (c)—$Ca_{23}$; (d), (e), (f)—$Ca_{14}$.

A typical example of the temperature evolution as the ATMC progresses is given in Figure 4 for a cluster with 23 atoms. Figure 4a shows the evolution of the temperature, which changed 247 times. Figure 4b depicts the corresponding changes in the average binding energy as the tempering process evolves. Figure 4c shows the correlation between tempering temperature and average binding energy along the tempering evolution. For some of the cluster sizes studied, the system evolves for a number of iterations, reaches a relatively low temperature where it seems to be trapped in a local minimum. Then the ATMC allows the system to overcome barriers and escape from such local minimum leading the system to excursion again to high temperature regions. Finally after more tempering events the system lands in the global minimum. One of such cases is shown in Figuers 4d, e, f for a $Ca_{14}$ cluster. As seen in Figure 4d, the cluster visits temperatures of about 50 K several times, and then rapidly takes excursions to regions of configuration space of higher binding energy (Fig. 4e). However, the cluster is able to hop out of these regions and excursion back to regions consistent with low temperatures. The cluster finally finds the global minimum, and the temperature collapses fast to 1 K. For this example there were 707 tempering events before ending the process. The correlation plot in Figure 4f shows clearly the successful efforts of the ATMC method to lead at low temperatures to the global minimum.

In Table III, third column, we have gathered results of the binding energy $E_N$ per atom, same results that are depicted in Figure 5a. The binding energy is defined as the TB electronic energy of a cluster of $N$ calcium atoms minus $N$ times the TB energy of one calcium atom. In Figure 5a, the TB results correspond to the empty triangles. For comparison, Table III, second column and the black triangles in Figure 5a are the TB energies of clusters with geometries borrowed from the Morse potential (parameter $\rho = 3.68$ adjusted for calcium[11]), which have been isotropically scaled to reach a minimum TB energy. It is clear that none of those Morse geometries is preferred over the configurations obtained with the ATMC.

The second difference of the TB energies obtained by our calculation is shown in Figure 5b. Peaks correspond to

**Table III.** Comparison of the binding energy of tight binding calcium clusters optimized with ATMC (second column) with the tight binding energy of clusters assuming a Morse structure with $\rho = 3.68$ (fifth column).

| $N$ | $-E_N/N$ (eV) from ATMC | Point group | $N$ | $-E_N/N$ (eV) from morse structure | Point group |
|---|---|---|---|---|---|
| 14 | 0.8684 | $C_{2v}$ | 14 | 0.8568 | $C_{2v}$ |
| 15 | 0.9178 | $C_{2v}$ | 15 | 0.8121 | $D_{6d}$ |
| 16 | 0.9319 | $C_s$ | 16 | 0.9158 | $C_s$ |
| 17 | 0.9680 | $C_s$ | 17 | 0.9455 | $C_{3v}$ |
| 18 | 0.9894 | $C_s$ | 18 | 0.9734 | $C_{5v}$ |
| 19 | 1.0266 | $D_{5h}$ | 19 | 1.0153 | $D_{5h}$ |
| 20 | 1.0471 | $C_{2v}$ | 20 | 1.0345 | $C_{2v}$ |
| 21 | 1.0700 | $C_{2v}$ | 21 | 1.0434 | $C_{2v}$ |
| 22 | 1.0804 | $C_s$ | 22 | 1.0689 | $C_s$ |
| 23 | 1.1138 | $C_{2v}$ | 23 | 1.0985 | $D_{3h}$ |
| 24 | 1.1211 | $C_{2v}$ | 24 | 1.1046 | $C_s$ |
| 25 | 1.1389 | $C_s$ | 25 | 1.1255 | $C_s$ |
| 26 | 1.1547 | $T_d$ | 26 | 1.1501 | $T_d$ |
| 27 | 1.1732 | $C_s$ | 27 | 1.1571 | $C_s$ |
| 28 | 1.1878 | $C_s$ | 28 | 1.1781 | $C_s$ |
| 29 | 1.2058 | $D_{3h}$ | 29 | 1.2009 | $D_{3h}$ |
| 30 | 1.2171 | $C_{2v}$ | 30 | 1.2038 | $C_{2v}$ |
| 31 | 1.2338 | $C_s$ | 31 | 1.2206 | $C_1$ |
| 32 | 1.2540 | $C_s$ | 32 | 1.2424 | $C_{2v}$ |

energetically preferred sizes because a size associated with a peak is more stable than the two neighboring sizes. It is interesting to note that there is an even-odd alternation where odd sizes are more stable than even sizes. Three of these sizes, 15, 21, and 23 show the most abrupt drop of peak height towards larger sizes. Because of that, these sizes can be called magic numbers. In this TB approach, the core electrons of Ca are frozen, and only the 2 valence electrons are considered. Therefore, the number of electrons corresponding to these magic number clusters is 30, 42, and 46, which are not consistent with shell closings of the jellium model (20, 40, 58, etc).

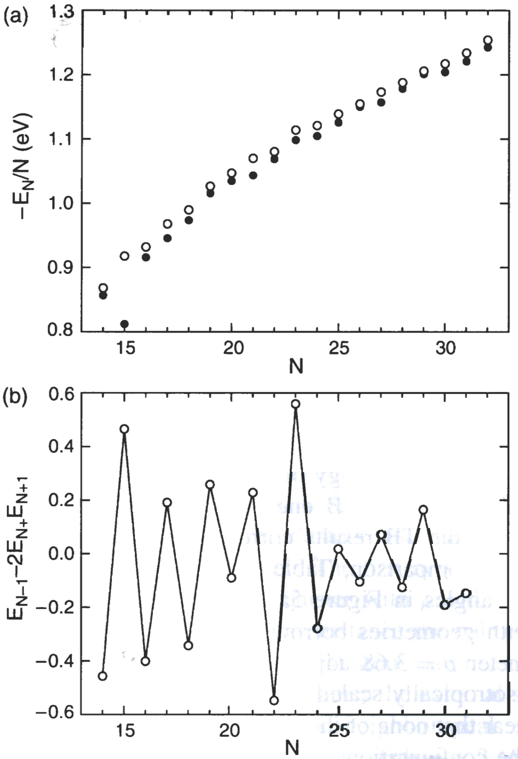

**Fig. 5.** Binding energy and stability pattern of calcium clusters versus size.

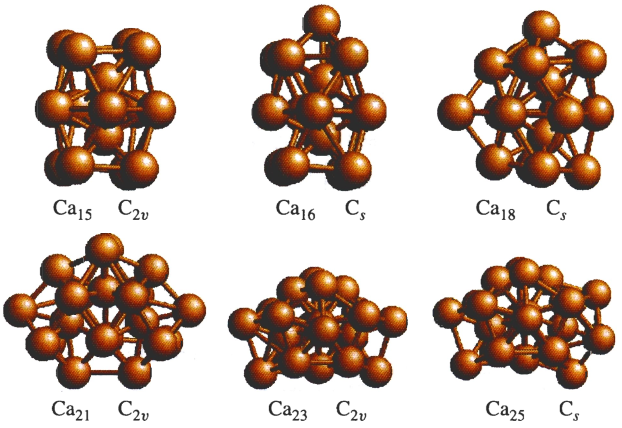

**Fig. 6.** Six new calcium cluster structures. $Ca_{15}$, $Ca_{21}$, and $Ca_{23}$ are magic numbers.

When analyzing closely the optimized cluster geometries, we find that all of them except for six are relaxed Morse structures in which bond lengths and angles accommodate somehow to adjust for the large surface to volume ratio. These six clusters, $Ca_{15}$, $Ca_{16}$, $Ca_{18}$, $Ca_{21}$, $Ca_{23}$, and $Ca_{25}$ depicted in Figure 6, have a structure not previously reported in the literature as energetically most stable under any model potential (Lennard Jones,[18] Morse,[12] Sutton-Chen,[19] TB-second-moment many body,[20, 21] Murrell Mottram,[22, 23] Dzugutov[24]). The three $C_{2v}$ magic number clusters are among the six new structures. The $Ca_{15}$ cluster is a pentagonal bipyramid with apex vertexes capped by two parallel squares. The $Ca_{23}$ cluster has a structure built on the elongated 19-atom icosahedron capped with one pentagonal pyramid to which two symmetrically opposed sides are decorated by dimers. The $Ca_{21}$ cluster is an incomplete 23-atom cluster in which two atoms are missing, the apex vertex atom and one from the pentagonal pyramid underneath.

TB also provides the one-electron quantum levels of the cluster valence band. It is interesting to note that these eigenvalues present a large energy gap between the highest occupied state and lowest unoccupied state of 0.63, 0.47, and 0.48 eV for the magic number clusters $Ca_{15}$, $Ca_{21}$, and $Ca_{23}$, respectively. However, the energy gap for all other sizes in the range studied is smaller, i.e., on the order of 0.05 to 0.1 eV. Figure 7 illustrates this effect. Eigenvalues are sorted by energy and numbered in increasing order from the bottom of the band. Figure 7 shows the distribution of TB eigenvalues in a ±1 eV band around the Fermi energy. Black circles identify occupied

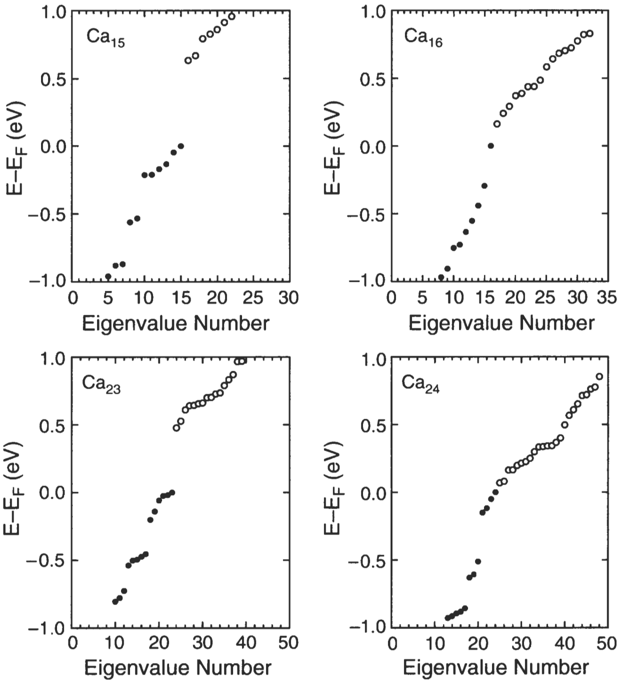

**Fig. 7.** Eigenvalues of $Ca_{15}$, $Ca_{16}$, $Ca_{23}$, $Ca_{24}$ near the Fermi energy.

states whereas white squares indicate the unoccupied states. Visually one sees that whereas the energy gap for $Ca_{15}$ is large, it is considerably smaller for $Ca_{16}$. The same effect is shown in Figure 7 for $Ca_{23}$ and $Ca_{24}$. Therefore, electronic effects are fundamental in the determination of the magic numbers in calcium clusters.

## 5. CRYSTALLIZATION OF A LENNARD JONES FLUID

A frequent problem of the Metropolis sampling in simulation of a structurally ordered state from a disordered state such as a liquid is the formation of defect-rich final structures in the case that the desired end phase is a crystalline solid. This problem arises because with this continuous path strategy the system makes excursions between two phases continuously along the simulation, which implies continuous crossing through regions of configuration space that have a mixed-phase type. Therefore in the transition from one phase to the other, one of the phases disassembles whereas the other assembles in a restructuring organized fashion. Additionally the simulation wastes time in regions of configuration space that do not contribute to the Metropolis sampling estimate. This process strongly favors the formation of defects in the

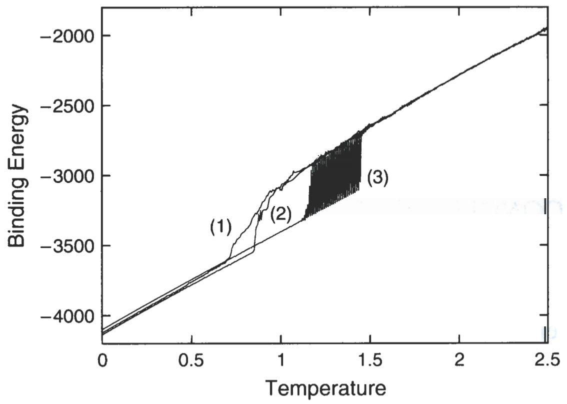

**Fig. 8.** Energy changes of the 500-atom Lennard Jones system along the tempering process for three values of the ATMC parameter: (1) $M_{\text{fixed}} = 50$; (2) $M_{\text{fixed}} = 100$; (3) $M_{\text{fixed}} = 200$.

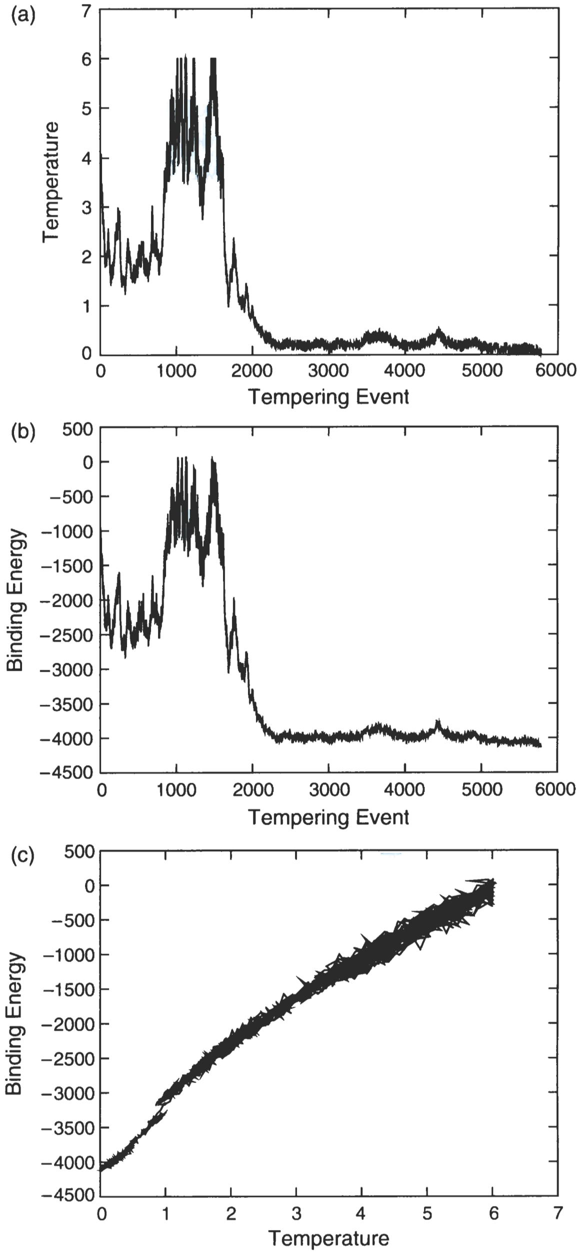

**Fig. 9.** Evolution of the temperature (a) and the energy (b) as a function of tempering event during crystallization of a LJ liquid; (c) correlation of temperature and energy along the tempering process. Shown is the case with $N = 500$ atoms.

final crystal. Another issue is the overlap problem in which the simulation is trapped in one of the phases and is unable to overcome the energy barriers to travel to the other phase. This last problem gives rise to systematic errors, which are difficult to eliminate. However, appropriate extended sampling techniques[25] will overcome the later. The ATMC is a convenient alternative when searching the structure of the ordered phase.

The ATMC was applied to evaluate the structural quality of the crystals when a liquid of LJ atoms solidifies. Periodic boundary conditions and computational box sizes with 108, 256, and 500 atoms were used. These systems were started from a liquid equilibrated at high temperature. Energies are reported in units of $\epsilon$, temperatures in units of $\epsilon/k_B$, and distances in units of $\sigma$. The ATMC parameters were $M_{\text{fixed}} = 100$ and $\ln a = -1.0$ for the three systems considered here. The selection of a good value for the first parameter is important. In Figure 8 we show the effect of this parameter on the tempering evolution for the case of $N = 500$. If the value of $M_{\text{fixed}}$ is too large or too small, the final energy at zero temperature is higher, indicating that some defects have formed. Also, if the parameter is too large, then the simulation wastes a long time in the region where the two phases coexist.

Figures 9a, b illustrate the evolution of temperature and energy as a function of tempering event for the case with $N = 500$. There were 5800 tempering events before crystallization. Depiction of how these two quantities are correlated is provided in Figure 9c. Once again, the correlation plot shows clearly two different linear regions associated to the two phases visited along the tempering evolution. When one compares the bulk evolution to the cluster evolution discussed in Section 3, it is clearly seen that in the case of the clusters (phases not sharply separated in configuration space) the ATMC recurs to changing the temperature up and down several times, whereas in the bulk case once the system finds its way towards low temperature, it stays there.

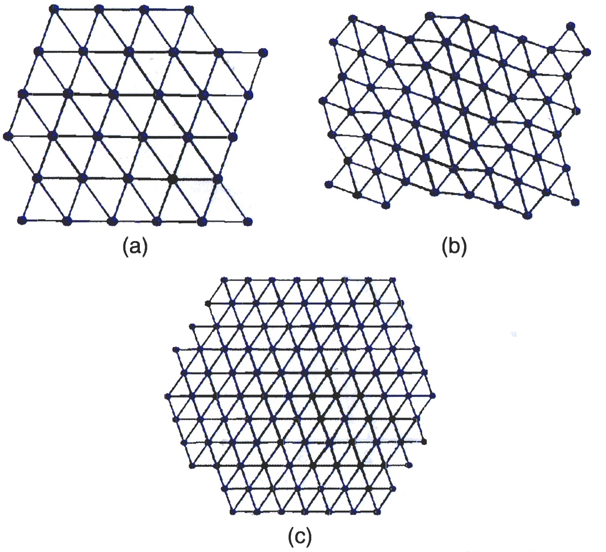

**Fig. 10.** Crystal structure after tempering. The view corresponds to the 111 face of a box with (a) 108 atoms; (b) 256 atoms; (c) 500 atoms.

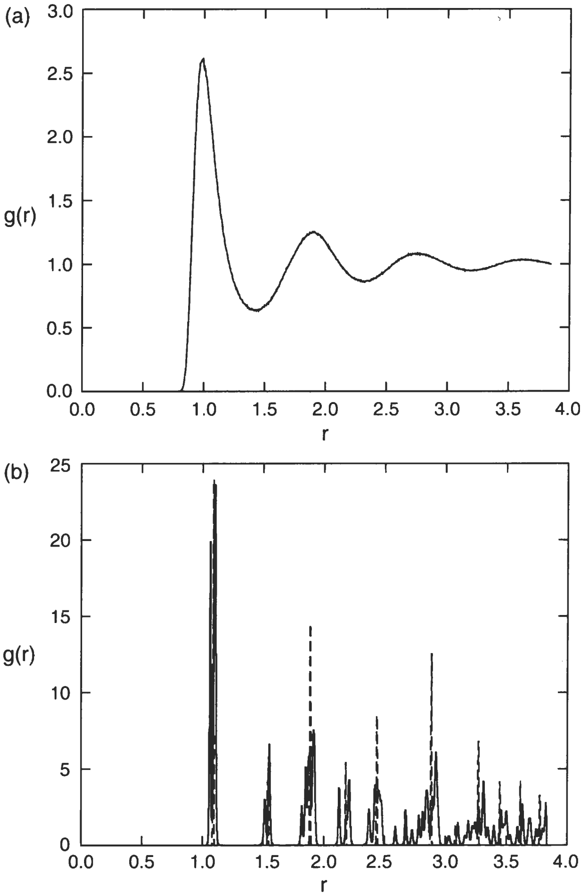

**Fig. 11.** Pair correlation function of the $N = 500$ crystal: (a) initial state at high temperature $T = 4$; (b) final state at low temperature $T = 0.001$.

In Figure 10 we give the (1,1,1) view of the final structure obtained for each of the three computational box sizes considered here. The crystals are almost perfect. More evidence is gained from Figure 11, which depicts the pair correlation function of the system with $N = 500$. At high temperature the equilibrated initial state at $T = 4$ is clearly a liquid and the final state at $T = 0.04$ is clearly the fcc lattice. The energy difference between a perfect fcc lattice oriented along the 0,0,1 axis of the computational box, and the energy of the tempered crystals are: 1.9%, 0.12%, 0.02% for the 500, 256, and 108 systems, respectively.

## 6. CONCLUSIONS

The computational framework of the adaptive tempering Monte Carlo is equally accessible for handling both, phenomenological particle potentials, and electronic structure approaches, to predict the global phase behavior leading to the most ordered phase of a system. This is particularly interesting for finite systems in the nanoscale regime where the nomination of two candidate phases is not a well defined concept. In this algorithm all anharmonicities are treated without approximation and one of the advantages of the ATMC is the possibility to thermally excite them through the tempering mechanism. The strategic advantage of this algorithm allows the nanosystems to escape from metastable states, which otherwise require extreme long-time dynamics indicating that the way in which the MC algorithm was engineered to move around configuration space is quite effective.

All together in this work we use the ATMC to find the sequence of growth, energetics, and stability of phenomenological atomic clusters modeled under the Morse potential and containing up to 155 atoms. Magic numbers and point group were obtained for two values of the Morse paramater $\rho = 3.0$ and 3.68. We also have found the preferred configuration and electronic structure of calcium clusters containing 14 to 32 atoms calculated within the tight binding approximation. This is an example of the possibilities that this algorithm presents to analyze systems from the perspective of quantum mechanics. A third example was to show the efficient crystallization obtained numerically under the ATMC which shortcuts the need of long times scales required in the atomic reorganization process intrinsic in the crystallization phenomenon.

There are yet other problems where this algorithm could result efficient to make the most of the information available in the configurational core of the system. We are presently exploring the awareness gained on finite size effects seen in the cluster calculations to tackle protein folding mechanisms of small proteins.

**Acknowledgments:** We acknowledge support of the Research Office of the Provost of George Mason University for the assistantship allocated to XD.

## References

1. E. Marinari and G. Parisi, *Europhys. Lett.* 19, 451 **(1992)**.
2. A. P. Lyubartsev, A. A. Martsinovski, S. V. Shevkunov, and P. N. Vorontsov-Velyaminov, *J. Chem. Phys.* 96, 1776 **(1992)**.
3. I. Nezbeda and J. Kolafa, *Molecular Simulation* 5, 391 **(1991)**.
4. G. M. Torrie and J. P. Valleau, *J. Comput. Phys.* 23, 187 **(1977)**.
5. B. A. Berg and T. Neuhaus, *Phys. Rev. Lett.* 68, 9 **(1992)**.
6. F. Wang and D. P. Landau, *Phys. Rev. Lett.* 86, 2050 **(2001)**.
7. Q. Yan, R. Faller, and J. J. de Pablo, *J. Chem. Phys.* 116, 8745 **(2002)**.
8. X. Dong, G. M. Wang, and E. Blaisten-Barojas, *Phys. Rev. B* 70, 205409 **(2004)**.
9. PGHPF™, The Portland Group, ST Microelectronics, Wilsonville, OR 97070.
10. Y. Sugita and Y. Okamoto, *Chem. Phys. Lett.* 314, 141 **(1999)**.
11. D. Wales, L. J. Munro, and J. P. K. Doye, *J. Chem. Soc. Dalton Trans.* 611 **(1996)**.
12. http://brian.ch.cam.ac.uk/CCD.html.
13. J. A. Northby, *J. Chem. Phys.* 87, 6166 **(1987)**.
14. J. C. Slater and G. F. Foster, *Phys. Rev.* 94, 1498 **(1954)**.
15. G. M. Wang, D. A. Papaconstantopoulos, and E. Blaisten-Barojas, *J. Phys. Chem. Solids* 64, 185 **(2003)**.
16. J. W. Mirick, C.-H. Chien, and E. Blaisten-Barojas, *Phys. Rev. A* 63, 023202 **(2001)**.
17. X. Dong, S. Gatica, and E. Blaisten-Barojas, *Computing Letters* 1 **(2006)**, in press.
18. D. J. Wales and J. P. K. Doye, *J. Phys. Chem. A* 101, 5111 **(1997)**.
19. J. P. K. Doye and D. J. Wales, *New J. Chem.* 22, 733 **(1998)**.
20. C. H. Chien, E. Blaisten-Barojas, and M. R. Pederson, *J. Chem. Phys.* 112, 2301 **(2000)**.
21. G. M. Wang, E. Blaisten-Barojas, A. E. Roitberg, and T. P. Martin, *J. Chem. Phys.* 115, 3640 **(2001)**.
22. J. N. Murrell and R. E. Mottram, *Mol. Phys.* 69, 571 **(1990)**.
23. J. E. Hearn and R. L. Johnson, *J. Chem. Phys.* 107, 4674 **(1997)**.
24. J. P. K. Doye and D. J. Wales, *Phys. Rev. Lett.* 86, 5719 **(2001)**.
25. J. R. Errington, *J. Chem. Phys.* 120, 3130 **(2004)**.

Received: 20 July 2005. Accepted: 24 August 2005.